Unfolded band structures of photonic quasicrystals and moiré superlattices

Yanbin Zhang, Zhiyuan Che,* Wenzhe Liu, Jiajun Wang, Maoxiong Zhao, Fang Guan, Xiaohan Liu, Lei Shi,† and Jian Zi‡
State Key Laboratory of Surface Physics, Key Laboratory of Micro- and Nano-Photonic Structures (Ministry of Education) and Department of Physics, Fudan University, Shanghai 200433, China

(Received 27 January 2022; revised 2 April 2022; accepted 5 April 2022; published 15 April 2022)

We apply the band-unfolding approach to explore the dispersions of different types of photonic quasiperiodic structures, including photonic quasicrystals that have high-rotational symmetry but lack translational symmetry, and moiré superlattices, which are a twist of two primary lattices. The band-unfolding approach provides a simple picture to get the band structure of such quasiperiodic structures, which can be directly compared with experimental results. We envision this approach will be a basic method for introducing the rich concepts of photonics in condensed-matter physics to photonic quasiperiodic systems.

DOI: 10.1103/PhysRevB.105.165304

I. INTRODUCTION

Photonic crystal, one of the most widely known artificial materials, has attracted continuous attention for its unique properties over the past few decades. Various optical phenomena such as light localization [1–3], complete band gap [4–6], negative refraction [7–9], anomalous dispersion [10,11], and bound states in the continuum [12–20] have been investigated, which provides a degree of freedom for practical applications [21–28]. Recently, the exploration of such fundamental concepts and exotic phenomena has extended to complex photonic systems, such as moiré superlattices and quasicrystals. These structures are considered quasiperiodic structures, which are the intermedium between photonic crystals and amorphous materials [29–31]. Photonic quasicrystals have properties beyond the periodic structures because of their high rotational symmetry, including topology states [32–36] and high-charge polarization vortices [37]. Moiré superlattices have been especially concerned with light localization [38–40], lasers [41], and slow light [42,43] for their magic-angle flat bands [44].

To capture the underlying photonic properties of these quasiperiodic systems, several theoretical models for dispersion calculation have been proposed, combined with the coupled-mode theory [45] and the transfer matrix method [46]. Another widely adopted investigating scheme of such systems is the supercell model [38,40,47–54] in which a certain block cluster (a supercell) in the target system is extracted and arranged periodically. By applying supercell model, the calculation method for periodic structures can be extended to the quasiperiodic structures. In general, moiré superlattices are classified into two types: Commensurate and incommensurate superlattice. The case of commensurate twisted angles of the two individual lattices naturally retains the periodicity, except that a smaller twisted angle is associated with the larger supercell [55,56] while, for the case of incommensurate twisted angles, moiré superlattices have no exact periodicity, similar to quasicrystals. It is necessary to construct their periodically approximate structure to obtain the supercell. Generally, to guarantee the accuracy of modeling, a larger supercell is required to approach the target structures [47]. However, the larger supercell corresponds to a tinier Brillouin zone (BZ), which will lead to difficulties in analyzing the dense folded band structures. The band-unfolding approach can remedy this problem, which has been successfully applied to alloy and impurity materials, van der Waals heterostructures, and quasicrystals in electronic systems [57–62].

In this paper, we apply the band-unfolding approach through the supercell model to photonic quasicrystals and moiré superlattices. Using this approach, the band structures of supercell BZ are unfolded into the primitive BZ constructed by the first-order diffraction spots. The unfolded band manifests the photonic properties of these quasiperiodic structures and can be directly compared with experimental measurements.

This paper is organized as follows: Details of the band-unfolding approach for the photonic structure are presented in Sec. II. Application examples of band-unfolding procedure are given in Sec. III. In Sec. IV, the comparison of simulation and experimental results are given; a brief conclusion of the paper is presented in Sec. V.

II. THEORY OF BAND-UNFOLDING APPROACH

We first present the theory behind band-unfolding approach based on supercell model, which has been described thoroughly for the electronic systems. This approach can be introduced to complex photonic systems. In this approach, the dense band structures distributed in the supercell BZ (SBZ) would be unfolded into an expected primitive BZ (PBZ). Figure 1 illustrates three different types of supercells and corresponding reciprocal lattices of photonic structures.

*zyche18@fudan.edu.cn
†lshi@fudan.edu.cn
‡jzi@fudan.edu.cn

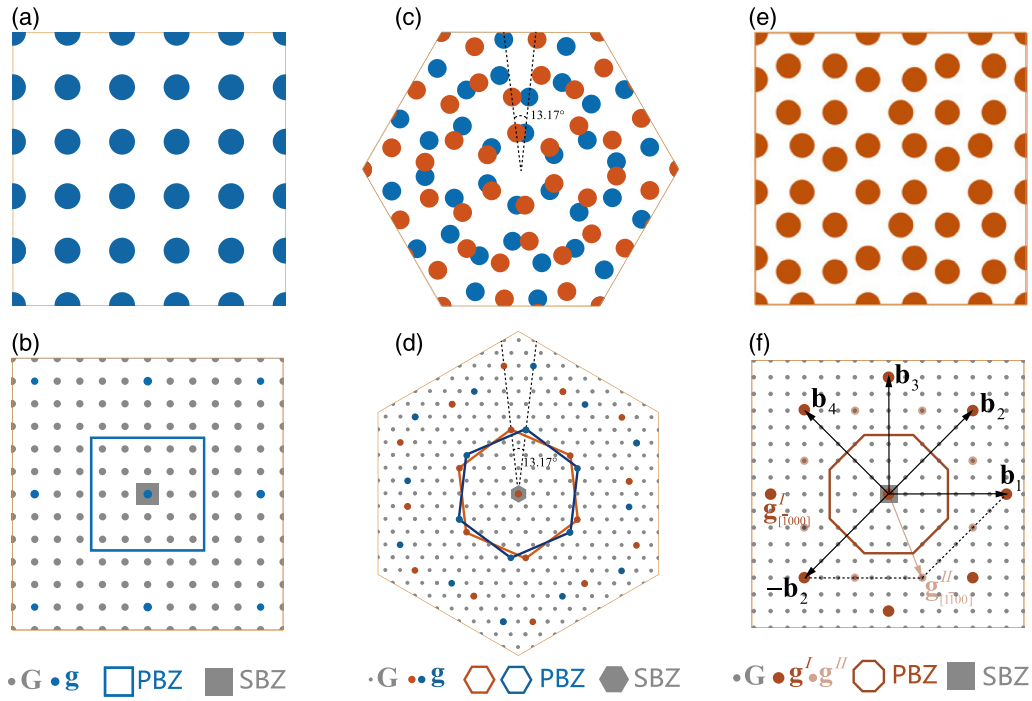

FIG. 1. (a) A 5×5 supercell of the square lattice. (c) A moiré-supercell of two twisted honeycomb lattices. (e) A square supercell of the eightfold quasicrystal. The corresponding reciprocal vectors (RVs), SBZs and PBZs are plotted in (b), (d), and (f). Four basic RVs $\mathbf{b}_l$, one first-order RV $\mathbf{g}^I_{[\bar{1}000]}$ and one second-order RV $\mathbf{g}^{II}_{[1\bar{1}00]}$ are marked in (f).

Figure 1(a) shows a 5×5 supercell of a square lattice, which is a repeating unit cell containing several primitive-cells. Figure 1(b) shows the reciprocal lattices of a supercell (**G**, gray dots), which correspond to a SBZ (gray square), and primitive cell (**g**, blue dots) associated with a PBZ (blue square). Similarly, a moiré supercell of two honeycomb lattices with a commensurate twisted angle is plotted in Fig. 1(c), and the corresponding reciprocal lattices of the moiré superlattice (**G**, gray dots) and two honeycomb lattices (**g**, blue and red dots) are plotted in Fig. 1(d). The SBZ and PBZ are denoted as gray, blue, and red hexagons. Figure 1(e) shows a square supercell of eightfold quasicrystals from periodic approximation (details as below), which exhibits quasiperiodicity in certain directions internally. Figure 1(f) shows the reciprocal lattices of supercell (**G**, gray dots) that correspond to a square SBZ, and quasiperiodic lattices (**g**, red dots) associated with a octagonal PBZ.

Here we denote the basic reciprocal vectors (RVs) of supercell lattices as $\{\mathbf{B}_l\}$, corresponding to lattice vectors $\{\mathbf{A}_l\}$. The arbitrary RV, **G**, can be denoted as

$$\mathbf{G} = \sum_l q_l \mathbf{B}_l, \ q_l \in \mathbb{Z}. \tag{1}$$

Similarly, the RV, **g**, of the primitive cell can be written as

$$\mathbf{g} = \sum_l p_l \mathbf{b}_l, \ p_l \in \mathbb{Z}, \tag{2}$$

where $\mathbf{b}_l$ is the basic RV associated with a set of primitive lattice vectors $\mathbf{a}_l$, which can be identified as integer multiples of $\{\mathbf{B}_l\}$ based on the geometrical relation. For periodic lattices, two or three vectors $\mathbf{b}_l$ are used for summation in the Eq. (2). For quasicrystals and moiré structures, at least four $\mathbf{b}_l$ are necessary. As an example, four $\mathbf{b}_l$ of eightfold quasicrystals with periodic approximation are marked as $\mathbf{b}_1$, $\mathbf{b}_2$, $\mathbf{b}_3$, and $\mathbf{b}_4$ in Fig. 1(f). To show the composition of $\mathbf{b}_l$ in **g**, we can mark **g** by a subscript as $\mathbf{g}_{[p_1 p_2 \ldots]}$. Meanwhile, we can classify the RVs in terms of order index, which is defined as $r = \sum_l |p_l|$, and labeled by their superscript as $\{\mathbf{g}^r\}$. Specifically, a first-order RV, $\mathbf{g}^I_{[\bar{1}000]}$, is marked in Fig. 1(f). And a second-order RV, $\mathbf{g}^{II}_{[1\bar{1}00]} = \mathbf{b}_1 - \mathbf{b}_2$, is illustrated.

It is worth noting that the PBZ of moiré structures and quasicrystals are different from that of periodic lattices which possess well-defined primitive cell. Obviously, the supercells of these complex structures cannot be seen as repeats of any primitive cell, especially the supercell of quasicrystals which is constructed from periodic approximation. But we can still define the PBZ in terms of intrinsic diffraction spots of the structure that originate from constructive wave interferences, even lack of periodicity [31,63]. For moiré structures, their PBZ consists of two twisted individual BZ corresponded to two sets of reciprocal lattices. For quasicrystal, the definition of PBZ is ambiguous. An ideal quasicrystal exhibits no strict BZ, while an effective BZ can be constructed by defining a polygon in reciprocal space, which is formed from the lines bisecting the basic RVs [63]. This BZ is referred to as the pseudo-BZ where the photonic dispersions govern the fundamental properties of whole structures. Considering that the pseudo-BZ is not directly related to the SBZ from supercell model, we naturally apply the basic RVs $\{\mathbf{b}_l\}$ of periodic approximant to construct PBZ for band-unfolding. To make a distinction, we denote $\{\widetilde{\mathbf{b}}_l\}$ as the basic RVs of the ideal quasicrystal. As the order of approximation increases,

those approximate vectors $\mathbf{b}_l$ approach $\widetilde{\mathbf{b}}_l$, the corresponding approximate structure approach ideal structure, and its PBZ approach the pseudo-BZ of ideal quasicrystal (see below).

The wave vector of SBZ (PBZ) can be denoted as $\vec{K}$ ($\vec{k}$), which obeys the unfolding relation:

$$\vec{k}_i = \vec{K} + \mathbf{G}_i. \tag{3}$$

Equation (3) indicates that one SBZ vector $\vec{K}$ can be unfolded to multiple PBZ vectors $\vec{k}$, which is marked by a subscript i, and this procedure is referred to as the unfolding of wave vector [59]. The eigenmodes of SBZ and PBZ are denoted by $|\vec{K}, \omega\rangle$ and $|\vec{k}, \omega\rangle$, respectively. According to the Bloch's theorm, one supercell mode $|\vec{K}, \omega\rangle$ can be written as

$$|\vec{K}, \omega\rangle = \mathbf{u}_{\vec{K}}(\mathbf{r})e^{i\vec{K}\cdot\mathbf{r}} = \widetilde{\mathbf{u}}_{\vec{K}+\mathbf{G}_i}(\mathbf{r})e^{i(\vec{K}+\mathbf{G}_i)\cdot\mathbf{r}}, \tag{4}$$

where $\widetilde{\mathbf{u}}_{\vec{K}+\mathbf{G}_i} = \mathbf{u}_{\vec{K}}e^{-i\mathbf{G}_i\cdot\mathbf{r}}$ with a vector $\mathbf{G}_i$. Equations (3) and (4) suggest that the mode $|\vec{K}, \omega\rangle$ lying in the SBZ may be represented as $|\vec{k}_i, \omega\rangle$ in PBZ if its eigenfield possesses Bloch character $\vec{k}_i$.

The probability of mode $|\vec{K}, \omega\rangle$ having the same Bloch character as a PBZ mode of wave vector $\vec{k}_i$ is defined by the spectral weight $P_{\vec{K}}(\vec{k}_i)$ [59,64],

$$P_{\vec{K}}(\vec{k}_i) = |\langle\vec{k}_i, \omega|\vec{K}, \omega\rangle|^2, \tag{5}$$

which is calculated by projecting $|\vec{K}, \omega\rangle$ on $|\vec{k}_i, \omega\rangle$ of a fixed $\vec{k}_i$. By adopting a plane-wave expansion for mode $|\vec{K}, \omega\rangle$, the spectral weight can be further written as

$$P_{\vec{K}}(\vec{k}_i) = \sum_{\mathbf{g}} |\mathbf{C}_{\vec{K}}(\mathbf{g}+\vec{k}_i - \vec{K})|^2, \tag{6}$$

where $\mathbf{C}_{\vec{K}}$ is the plane wave coefficient. Recalling Eqs. (3) and (4), $\mathbf{C}_{\vec{K}}$ is obtained by

$$\begin{aligned}\mathbf{C}_{\vec{K}}(\mathbf{g} + \vec{k}_i - \vec{K}) &= \int d^3r\mathbf{u}_{\vec{K}}(\mathbf{r})e^{-i(\mathbf{g}+\mathbf{G}_i)\cdot\mathbf{r}} \\ &= \int d^3r\widetilde{\mathbf{u}}_{\vec{K}+\mathbf{G}_i}(\mathbf{r})e^{-i\mathbf{g}\cdot\mathbf{r}},\end{aligned} \tag{7}$$

where the integration is performed over the supercell. The second equality in Eq. (7) indicates the significance of nontrivial $P_{\vec{K}}(\vec{k}_i)$, which is the Fourier transform pattern of $\widetilde{\mathbf{u}}_{(\vec{K}+\mathbf{G}_{nm})}$ has some diffraction spots overlapped with PBZ lattice vectors $\mathbf{g}$, as illustrated inthe Fig. 1 of Ref. [37].

Once thousands of SBZ eigenmodes and corresponding spectral weights for certain vectors $\mathbf{G}_i$ have been calculated, the band structures laying in the SBZ will be represented in the PBZ, called band unfolding. In fact, the only unknown condition for calculation of the spectral weight in Eq. (7) is the geometrical relations between RVs $\mathbf{g}$ and vectors $\mathbf{G}$ or, equivalently, the relation of the basic vectors $\mathbf{b}_i$ to $\mathbf{B}_i$. Thus, when we apply the band-unfolding approach to specific photonic systems, a key step is to determine these geometrical relations of the basic RVs of SBZ and PBZ. The following section will demonstrate the construction of those key relations for photonic quasicrystals and moiré structures.

III. APPLICATIONS

The implementation of the band-unfolding approach can be summarized in the following steps: (1) Construct the target structures with periodicity in real space. (2) Extract the supercell and determine the relation between $\mathbf{g}$ and vectors $\mathbf{G}$ in reciprocal space. (3) Obtain the supercell eigenmodes from numerical simulations (using software COMSOL MULTIPHYSICS). (4) Caluclate the spectral weights. (5) Represent the unfolded band structures. Note that for a 2D photonics systems, the eigenfield E_z (H_z) of supercell modes is used to calculate the spectral weight of TM (TE) modes. Especially, for quasi-2D systems, like photonic slabs, the eigenfield E_z (H_z) in the $x-y$ plane is also used to calculate the spectral weight of TM-like (TE-like) modes.

A. Photonic quasicrystals

For the quasicrystals, the lack of translational symmetry makes it impossible to define a unit cell for band calculation. The general treatment is to select a supercell containing the features of quasicrystals and impose periodic boundary conditions to investigate the approximate band structure. In other words, we need to find a rational supercell as the repeating unit-cell to construct the periodically approximate structure of the quasicrystals. Therefore, the selection of supercells is particularly important, which requires an approximation criteria to evaluate whether the approximate structure is close to ideal quasicrystals.

We begin with the construction of an ideal quasicrystal and its approximate structures. A simple method to get the spatial configuration of an ideal quasicrystal with two component dielectric materials is the density-wave method based on the reciprocal lattices [48–50]. In this method, the distribution of dielectric constant is given by

$$\varepsilon(\mathbf{r}_{//}) = \begin{cases}\varepsilon_1, & \mathrm{Re}[\rho(\mathbf{r}_{//})] > \mathrm{t} \\ \varepsilon_0, & \mathrm{Re}[\rho(\mathbf{r}_{//})] < \mathrm{t},\end{cases} \tag{8}$$

where $\mathbf{r}_{//}$ is the in-plane position vector and t is a numerical threshold to tune the filing ratio. The so-called density wave is the sum of plane waves,

$$\rho(\mathbf{r}_{//}) = \sum_r \sum_m A_m^r e^{i\mathbf{g}_m^r\cdot\mathbf{r}_{//}+\phi_m^r}, \tag{9}$$

where phases ϕ_m^r and amplitude A_m^r correspond to mth RVs of r order, $\mathbf{g}_m^r$. The first two sets vector of $\{\mathbf{g}^I\}$ and $\{\mathbf{g}^{II}\}$ are generally used. As an example, a structure of 12-fold photonic quasicrystals with two components (refractive index of 1 and 1.5) constructed by this method is shown in Fig. 2(a). The corresponding reciprocal lattices are plotted in Fig. 2(b). The basic RVs are defined by

$$\widetilde{\mathbf{b}}_l = \frac{2\pi}{a_0}\left(\cos\frac{(l-1)\pi}{6}, \sin\frac{(l-1)\pi}{6}\right); l = 1, \ldots, 6, \tag{10}$$

where the meaning of parameter a_0 is the average lattice constant in the direction of six basic RVs. These vectors of $\{\mathbf{g}^I\}$ and $\{\mathbf{g}^{II}\}$ are denoted by blue and green rings in Fig. 2(b).

Then we consider constructing periodic approximants of the quasicrystal. The complexity of the quasicrystal in real space makes this issue not easily solvable. Considering the

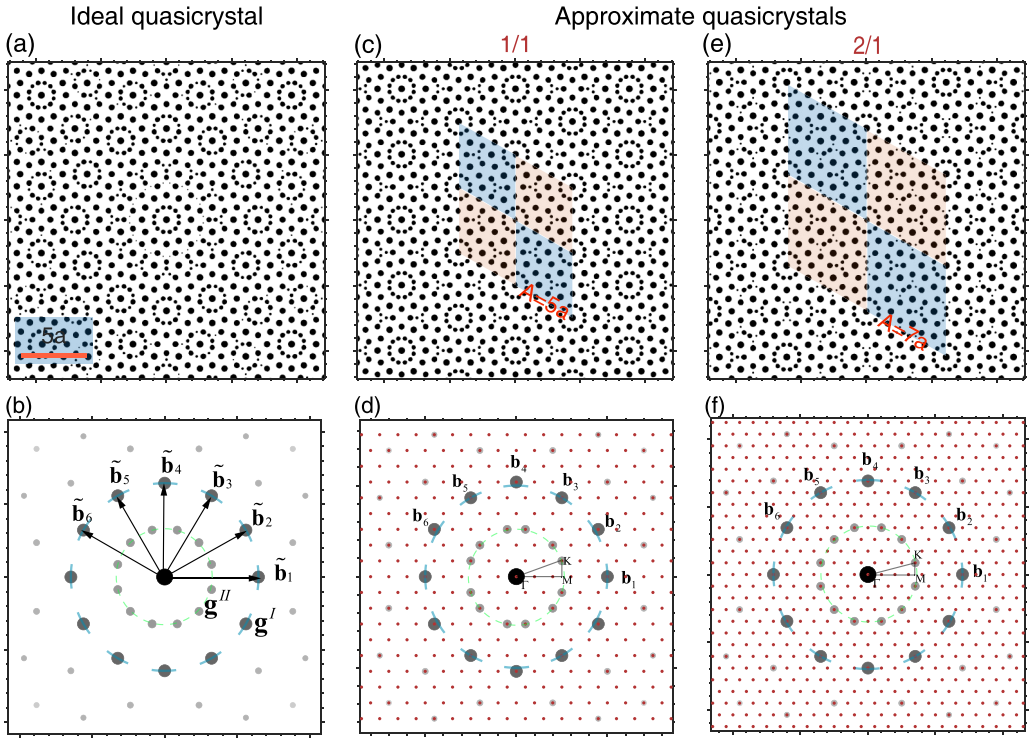

FIG. 2. Photonic quasicrystal and its periodic approximants. (a) A 2D 12-fold quasicrystal structure. (b) Reciprocal lattices. Six basic reciprocal vectors are denoted by black arrows. (c), (d) Periodic approximants and corresponding reciprocal lattices of $p_n/q_n = 1/1$. (e), (f) Periodic approximants and corresponding reciprocal lattices of $p_n/q_n = 2/1$. The suprecell for each approximant is marked as rhombuses. The modified basic reciprocal vectors are also marked as same as in (b).

role of RVs in the density-wave method, we may complete the construction of periodic approximants by modifying the RVs. The key features of quasicrystals in the reciprocal space are completely described by the basic RVs, which not only reflect their rotational symmetry but also lead to the lack of periodicity. Therefore, a set of modified basic RVs is required to possess not only the rotational symmetry of quasicrystals even approximately, but also the periodicity. In other words, the core of construction of the periodic approximants is to choose a set of basic RVs in a periodic lattice to approach that of the ideal quasicrystal. Specifically, these modified vectors are generated by changing the norm or direction of $\tilde{\mathbf{b}}_l$.

To form the periodic approximants of 12-fold quasicrystals, we can choose their basic RVs in the hexagonal lattices. This gives a better approximant than that from square, rectangular, or other periodic lattices, due to six being the largest divisor of 12- and sixfold rotational symmetry being closer to 12-fold symmetry. A set of basic RVs, $\mathbf{b}_l$, is chosen as

$$\begin{aligned}
\mathbf{b}_1 &= (2p_n + 3q_n)\mathbf{B}_1, \\
\mathbf{b}_3 &= (2p_n + 3q_n)\mathbf{B}_2, \\
\mathbf{b}_5 &= (2p_n + 3q_n)(\mathbf{B}_2 - \mathbf{B}_1), \\
\mathbf{b}_2 &= (p_n + 2q_n)(\mathbf{B}_1 + \mathbf{B}_2), \\
\mathbf{b}_4 &= (p_n + 2q_n)(2\mathbf{B}_2 - \mathbf{B}_1), \\
\mathbf{b}_6 &= (p_n + 2q_n)(\mathbf{B}_2 - 2\mathbf{B}_1),
\end{aligned} \tag{11}$$

where $\mathbf{B}_1 = 4\pi(1/\sqrt{3}, 0)/A$ and $\mathbf{B}_2 = 2\pi(1/\sqrt{3}, 1)/A$ are basic RVs of the hexagonal lattice, and $\tau_n = p_n/q_n = 1/1, 2/1, 5/3, 7/4, 19/11\ldots$, which is from continued fraction expansion of the irrational number $\sqrt{3}$. As $n \to \infty$, the fraction series $\tau_n \to \sqrt{3}$, these approximate vectors $\mathbf{b}_l$ approach $\tilde{\mathbf{b}}_l$ in Eq. (10), and the approximants approach the ideal quasicrystals. It should be noted that norms of $\mathbf{b}_2$, $\mathbf{b}_4$, and $\mathbf{b}_6$ are not equal to that of $\mathbf{b}_1$, $\mathbf{b}_3$, and $\mathbf{b}_5$, which approximately reflect the rotational symmetry of a 12-fold quasicrystal. The resulting periodic approximants will possess the periodicity of a hexagonal lattice and determine a rhombic supercell with a sharp angle of $\pi/3$ and side length of $A = a(2p_n + 3q_n)$ with $a = a_0/\sin(\pi/3)$.

Substituting Eq. (11) instead of Eq. (10) into Eq. (2), we can easily obtain the periodically approximate structure of the quasicrystal by using formulas of the density-wave method. Structures of the first two order approximants $p_n/q_n = 1/1$ and $2/1$ for 2D 12-fold photonic quasicrystal are plotted in Figs. 2(c) and 2(e), and corresponding supercells are marked as rhombuses. Compared with the structure in Fig. 2(a), those structures in Figs. 2(c) and 2(e) possess supercells of different sizes, while their approximation is easier to be evaluated by the corresponding basic RVs. Figures 2(d) and 2(f) show the basic RVs of a 12-fold quasicrystal of approximant $p_n/q_n = 1/1$ and $2/1$. The red grid points denote the reciprocal lattices of the hexagonal lattice, $\{\mathbf{G}\}$. The first-order reciprocal lattices, $\{\mathbf{g}^I\}$, and second-order ones, $\{\mathbf{g}^{II}\}$, are marked by blue and green rings—same as in Fig. 2(b). Obviously, these vectors in Fig. 2(f) are closer to that in Fig. 2(b) than in Fig. 2(d). The similar periodic approximations for fivefold, tenfold, and eightfold quasicrystals and corresponding vector relations can be found in Refs. [47,49,65].

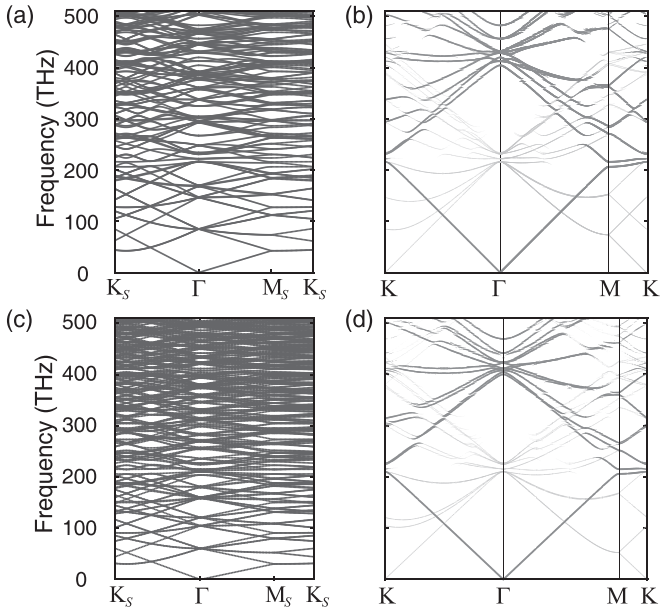

FIG. 3. Band structures of 2D 12-fold photonic quasicrystals. (a) Folded band structures of TM modes applied supercell calculations of $p_n/q_n = 1/1$. (b) Unfolded band structures in the PBZ. (c), (d) Folded and unfolded band structures of $p_n/q_n = 2/1$.

Figure 3(a) shows the band structures of TM modes in the SBZ calculated from the supercell of approximants $p_n/q_n = 1/1$. The unfolded band structures in the PBZ are shown in Fig. 3(b). Similarly, the SBZ band structures and the corresponding unfolded band structures for approximants $p_n/q_n = 2/1$ are shown in Figs. 3(c) and 3(d). The two results show good agreement except for slight differences in details, which indicates these periodic approximants appropriate for investigating the band structures of quasicrystals. As the order of approximation increases, the unfolded band structures converge to the dispersion of the ideal quasicrystal. In general, the second-order approximant is enough for the accuracy and appropriate simulation times. In addition, the scattering strength of RVs $\{\mathbf{g}^I\}$ is greater than that of $\{\mathbf{g}^{II}\}$ (denoted by sizes of diffraction spots); this contrast can be reflected in the corresponding band structures by different gray scales. In Figs. 3(b) and 3(d), the unfolded band structures of $\{\mathbf{g}^I\}$ and $\{\mathbf{g}^{II}\}$ are marked by dark and light gray, respectively. This point can also be verified experimentally in the extinction spectrum.

B. Photonic Moiré superlattices

After applying the band-unfolding approach to photonic quasicrystals, we rationally extend this approach into another kind of complex photonic structures—-moiré superlattices, due to the fact that a quasicrystal can be seen as a special moiré superlattice [56]. Moiré superlattices are structures composed of two or more identical lattices with a relative in-plane twisted angle. For some special twisted angles, moiré superlattice exhibits periodicity, but the length scale of its unit-cell is much larger than that of original lattices, known as commensurate moiré supercells [e.g., Fig. 1(c)]. When no periodicity is retained, moiré superlattices are incommensurate.

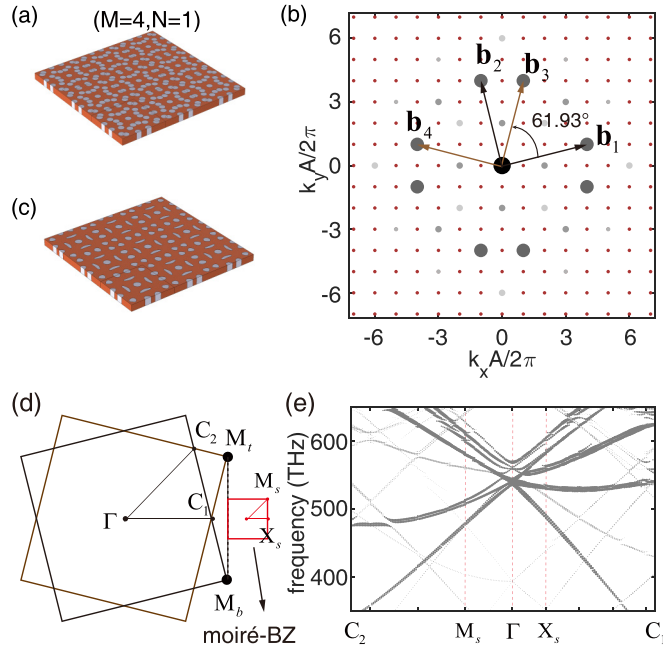

FIG. 4. Example of photonic moiré superlattice. (a) A monolayer slab structure of commensurate moiré superlattices of $(M = 4, N = 1)$. (b) Two sets of basic reciprocal vectors of square lattices with a twisted angle 61.93°. Red points present the reciprocal lattices of moiré superlattice. (c) A moiré structure obtained from density-wave method. (d) The PBZ of two twisted lattices and SBZ (red square, namely, moiré-BZ). (e) Unfolded band structure for supercell calculation of TM-like modes.

For the commensurate case, we consider that the moiré superlattice consists of two square lattices. Its basic vectors can be defined by [56,66]

$$\mathbf{A}_1 = M\mathbf{a}_1 + N\mathbf{a}_2, \quad \mathbf{A}_2 = -N\mathbf{a}_1 + M\mathbf{a}_2, \tag{12}$$

where M and N are integers; $\mathbf{a}_1$ and $\mathbf{a}_2$ are the lattice vectors of a square lattice with the lattice constant a. The side length of corresponding square moiré supercell is $A = \sqrt{M^2 + N^2}a$ and the twisted angle is then written as

$$\cos\theta = \frac{2MN}{M^2 + N^2}. \tag{13}$$

According to the reciprocity of real lattices and reciprocal lattices, we can easily obtain the relation of basic RV between moiré superlattice and original lattices. The basic RVs of the moiré superlattices are denoted as $\mathbf{B}_1 = 2\pi(1, 0)/A$, $\mathbf{B}_2 = 2\pi(0, 1)/A$. Based on Eq. (12), the geometrical relations similar to Eq. (11) are given by

$$\begin{aligned} \mathbf{b}_1 &= M\mathbf{B}_1 + N\mathbf{B}_2, \quad \mathbf{b}_2 = -N\mathbf{B}_1 + M\mathbf{B}_2, \\ \mathbf{b}_3 &= N\mathbf{B}_1 + M\mathbf{B}_2, \quad \mathbf{b}_4 = -M\mathbf{B}_1 + N\mathbf{B}_2, \end{aligned} \tag{14}$$

where $\mathbf{b}_1$ and $\mathbf{b}_2$ denote basic RVs of one square lattices; $\mathbf{b}_3$ and $\mathbf{b}_4$ denote that of other lattices.

Figure 4(a) is example of a monolayer moiré structure for a square lattice of $M = 4, N = 1$. Two arrays of holes are arranged on a 2D dielectric slab (refractive index $n = 2$,

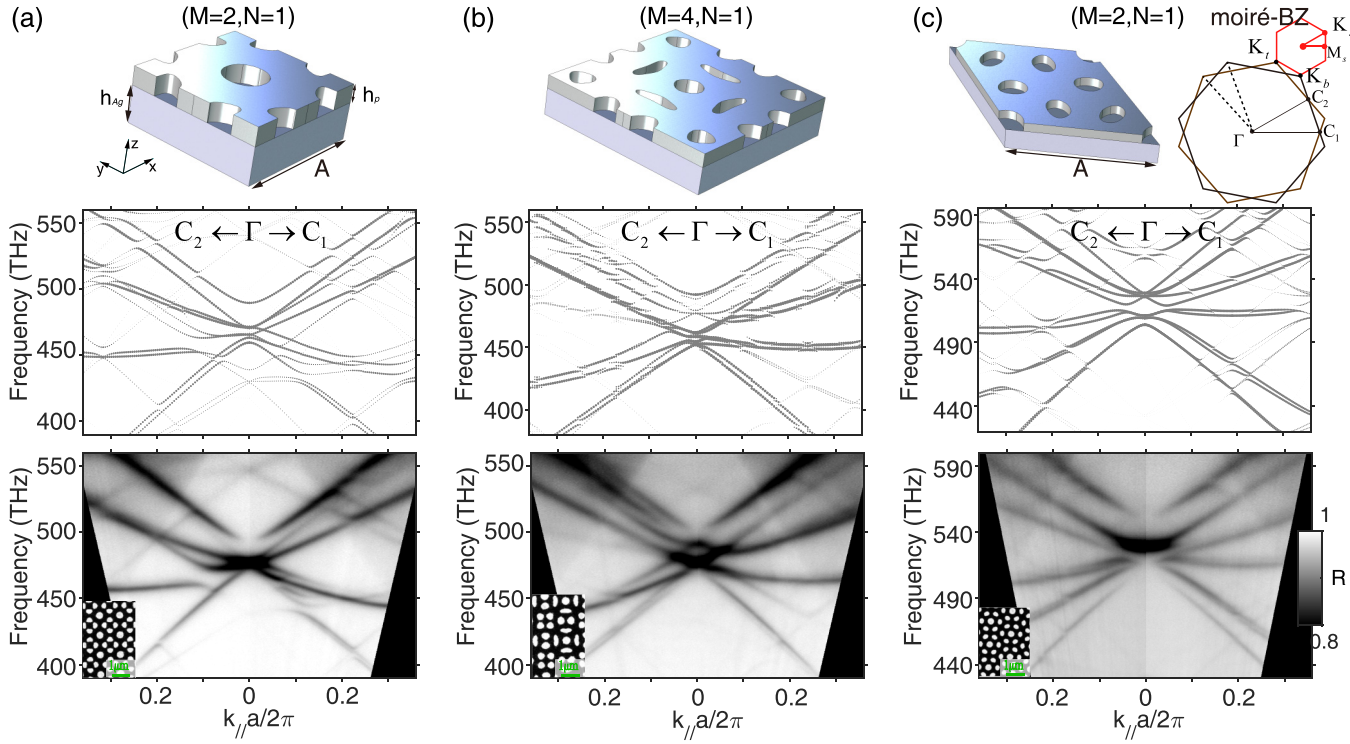

FIG. 5. Comparison of calculated and measured band structures. Moiré superlattices of $M = 2, N = 1$ (a) and $M = 4, N = 1$ (b) for square lattice, and $M = 2, N = 1$ (c) for hexagonal lattice. The supercells (top row) are used to calculate the eigenstates of SPP modes for these moiré superlattices. The calculated band structures (second row) are consistent with these measured results (third row). The corresponding SEM images are shown in the bottom-left corner.

thickness 100 nm). In fact, by applying Eqs. (8) and (9), a structure with the same moiré feature can be constructed, as shown in Fig. 4(c). Figure 4(b) shows the basic RVs of these structures in Figs. 4(a) and 4(c). The red grid points indicate the reciprocal lattices of the moiré superlattices, **G**. In Fig. 4(d), the two large squares represent the PBZ and red square is the SBZ which is also called the moiré-BZ or mini-BZ in some Refs. [41,45]. The unfolded band structures of TM-like modes in the PBZ are plotted in Fig. 4(e). Clearly, bands along the direction of $\Gamma - X_S$ are unfolded into $\Gamma - C_1$ and bands along the direction of $\Gamma - M_S$ are unfolded into $\Gamma - C_2$, where C_1 and C_2 are the cross points of two PBZ.

For the incommensurate superlattice, a periodically approximate supercell is required, similarly to quasicrystals. To construct the supercell of incommensurate superlattice, the stretching or compression of one lattice is generally required, which has been studied in Refs. [62,67]. A special case of incommensurate moiré superlattice consists of two hexagonal lattices twisted by 30° which possesses 12-fold rotational symmetry. Its approximate supercell can be generated using Eq. (11) for the similarity between this moiré structure and the 12-fold quasicrystal. In fact, basic RVs of $\mathbf{b}_1, \mathbf{b}_3$, and $\mathbf{b}_5$ in Eq. (11) correspond to a set of hexagonal lattices, while $\mathbf{b}_2, \mathbf{b}_4$, and $\mathbf{b}_6$ correspond to another set of hexagonal lattices with twisted angle of 30°, and their norm is stretched or compressed, noting that their norm is not equal to the norm of $\mathbf{b}_1$. Thus, $\mathbf{B}_1$ and $\mathbf{B}_2$ are the basic RVs of approximate moiré superlattice with a supercell. This method of constructing the supercell is easily generalized to arbitrary twisted angles of incommensurate moiré superlattices. After that, the band-unfolding approach can be directly applied to incommensurate moiré superlattices.

IV. COMPARISON WITH EXPERIMENTAL RESULTS

To verify the validity of the above methods, we experimentally focused on the 2D plasmonic structures of the moiré superlattices and quasicrystals to compare their unfolded band structures with the measured results. Using electron-beam lithography, the plasmonic structures are fabricated by spin-coated polymethyl methacrylate (PMMA) thin film on metallic substrate with air holes of moiré superlattices or quasicrystal patterns. The metallic substrate is a 200-nm-thick silver film evaporated on a silicon substrate, and the PMMA film (refractive index of 1.5) is about 90 nm thick. Their measured band structures, which are the angle-resolved reflectance spectrums obtained from our homemade momentum-space imaging spectroscopy system [68], are, respectively, shown in the third row of Figs. 5 and 6(b) with corresponding SEM images.

Figure 5 shows examples for commensurate moiré structures of square and hexagonal lattices. The supercells of a plasmonic moiré structure used to calculate the eigenmodes are plotted in the top row of the Fig. 5. The generation of an in-plane moiré pattern is similar to that of Fig. 4(c). Two examples of a square lattice of $M = 2, N = 1$ and $M = 4, N = 1$ are shown in Figs. 5(a) and 5(b). Similar to the twisted square lattices, we can obtain the relations of two sets of reciprocal basic vector for hexagonal lattices: $\mathbf{b}_1 = M\mathbf{B}_1 + N\mathbf{B}_2$, $\mathbf{b}_2 = -N\mathbf{B}_1 + (M+N)\mathbf{B}_2$,

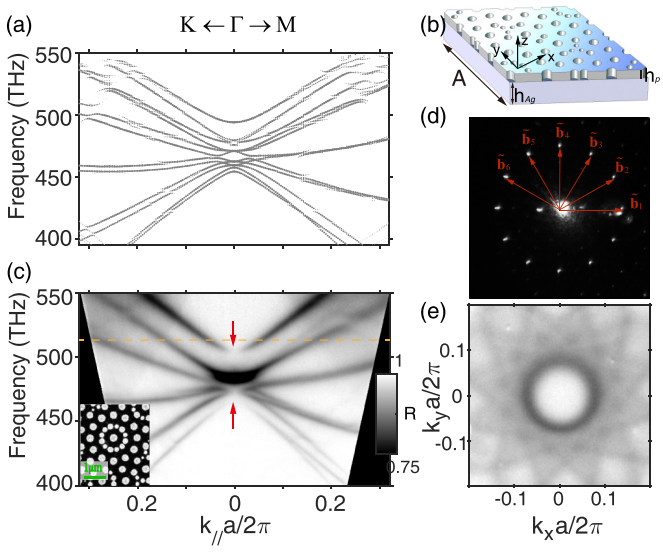

FIG. 6. Comparison of calculated and measured band structures of 12-fold plasmonic quasicrystal structure. (a) Calculated band structure of SPP modes along $\Gamma - \mathrm{K}$ and $\Gamma - \mathrm{M}$. (b) Schematic view of supercell for approximant $p_n/q_n = 2/1$. (c) Measured band structure with its SEM image in bottom-left corner. (d) Diffraction pattern, six basic RVs are indicated as red arrows. (e) Measured isofrequency contour at 570 nm [marked as dotted orange line in (c)].

$\mathbf{b}_3 = N\mathbf{B}_1 + M\mathbf{B}_2$, and $\mathbf{b}_4 = -M\mathbf{B}_1 + (M+N)\mathbf{B}_2$, where $\mathbf{B}_1$ and $\mathbf{B}_2$ are basic vectors of hexagonal lattice with side length $A = a\sqrt{M^2 + N^2 + MN}$ [60]. The results of $M = 2, N = 1$ moiré structures for a twisted hexagonal lattice are shown in Fig. 5(c). The hexagonal BZs of two regular lattices with twisted angle 21.79°and moiré-BZ of the superlattice are plotted in the top-right corner. We can find good agreement between these unfolded band structures (second row) and measured band structures (third row).

We also show the example for plasmonic quasicrystals of 12-fold rotational symmetry. The calculated band structures that is obtained from the first-order approximation $p_n/q_n = 2/1$ of the 12-fold quasicrystals with a supercell [Fig. 6(b)] are plotted in Fig. 6(a). The measured band structures from angle-resolved reflectance spectrum are plotted in Fig. 6(c) with its SEM image in bottom-left corner. The comparison shows that calculations agree well with measurements. In addition, the spectrum shows the existence of several diminishing points at the Γ point, as pointed out by red arrows in Fig. 6(c). The disappearance indicates that those modes are hardly excited and are nearly decoupled from the free space. In fact, those modes are quasibound states in the continuum, i.e., leaky modes with high-quality factor and associate with the polarization vortex in the momentum space of radiation far-field, which is theoretically discussed in Ref. [37]. Meanwhile, the high-rotational symmetry of quasicrystals predicts the manifestation of isotropy [48]. The diffraction pattern of this structure is plotted in Fig. 6(d), and the six basic RVs are indicated as red arrows. We can observe the near circular isofrequency contour near the Γ point, as shown in Fig. 6(e).

V. CONCLUSIONS

In conclusion, we have employed a general approach to investigate quasiperiodic structures and moiré superlattices, which has effectively combined the techniques of supercell calculation and band unfolding. Such an approach not only provides a global perspective in a regular-defined BZ to analyze the photonic dispersions of those complex systems but also provides a better interface for comparison between experimental measurements and numerical calculations. Furthermore, this approach can be employed to study the topological properties of complex photonic structures that have recently attracted enormous attention fueled by rapid progress made in singular optics, topological photonics, including singularities of phase and polarization of radiation far-field, and phase transition from periodic to moiré superlattice and quasiperiodic systems.

ACKNOWLEDGMENTS

The work was supported by the China National Key Basic Research Program (No. 2016YFA0301103, No. 2016YFA0302000, and No. 2018YFA0306201) and the National Science Foundation of China (No. 11727811, No. 91750102, and No. 91963212). L.S. was further supported by the Science and Technology Commission of Shanghai Municipality (No. 19XD1434600, No. 2019SHZDZX01, and No. 19DZ2253000).

Y.Z. and Z.C. contributed equally to this work.

[1] S. John, Phys. Rev. Lett. **58**, 2486 (1987).
[2] R. D. Meade, K. D. Brommer, A. M. Rappe, and J. D. Joannopoulos, Phys. Rev. B **44**, 13772 (1991).
[3] E. Yablonovitch, T. J. Gmitter, R. D. Meade, A. M. Rappe, K. D. Brommer, and J. D. Joannopoulos, Phys. Rev. Lett. **67**, 3380 (1991).
[4] E. Yablonovitch, J. Opt. Soc. Am. B **10**, 283 (1993).
[5] J. D. Joannopoulos, P. R. Villeneuve, and S. Fan, Nature (London) **386**, 143 (1997).
[6] J. D. Joannopoulos, S. G. Johnson, J. N. Winn, and R. D. Meade, *Photonic Crystals: Molding the Flow of Light* (Princeton University Press, Princeton, 2011)
[7] M. Notomi, Phys. Rev. B **62**, 10696 (2000).
[8] J. B. Pendry, Phys. Rev. Lett. **85**, 3966 (2000).
[9] E. Cubukcu, K. Aydin, E. Ozbay, S. Foteinopoulou, and C. M. Soukoulis, Nature (London) **423**, 604 (2003).
[10] T. Baba, Nat. Photon. **2**, 465 (2008).
[11] X. Huang, Y. Lai, Z. H. Hang, H. Zheng, and C. T. Chan, Nat. Mater. **10**, 582 (2011).
[12] C. W. Hsu, B. Zhen, J. Lee, S.-L. Chua, S. G. Johnson, J. D. Joannopoulos, and M. Soljačić, Nature (London) **499**, 188 (2013).
[13] B. Zhen, C. W. Hsu, L. Lu, A. D. Stone, and M. Soljačić, Phys. Rev. Lett. **113**, 257401 (2014).

[14] C. W. Hsu, B. Zhen, A. D. Stone, J. D. Joannopoulos, and M. Soljačić, Nat. Rev. Mater. **1**, 16048 (2016).

[15] H. M. Doeleman, F. Monticone, W. den Hollander, A. Alù, and A. F. Koenderink, Nat. Photon. **12**, 397 (2018).

[16] Y. Zhang, A. Chen, W. Liu, C. W. Hsu, B. Wang, F. Guan, X. Liu, L. Shi, L. Lu, and J. Zi, Phys. Rev. Lett. **120**, 186103 (2018).

[17] W. Chen, Y. Chen, and W. Liu, Phys. Rev. Lett. **122**, 153907 (2019).

[18] W. Ye, Y. Gao, and J. Liu, Phys. Rev. Lett. **124**, 153904 (2020).

[19] X. Yin, J. Jin, M. Soljačić, C. Peng, and B. Zhen, Nature (London) **580**, 467 (2020).

[20] T. Yoda and M. Notomi, Phys. Rev. Lett. **125**, 053902 (2020).

[21] S.-Y. Lin, E. Chow, V. Hietala, P. R. Villeneuve, and J. D. Joannopoulos, Science **282**, 274 (1998).

[22] J. C. Knight, Nature (London) **424**, 847 (2003).

[23] O. Painter, R. K. Lee, A. Scherer, A. Yariv, J. D. O'Brien, P. D. Dapkus, and I. Kim, Science **284**, 1819 (1999).

[24] J. Jin, X. Yin, L. Ni, M. Soljačić, B. Zhen, and C. Peng, Nature (London) **574**, 501 (2019).

[25] B. Wang, W. Liu, M. Zhao, J. Wang, Y. Zhang, A. Chen, F. Guan, X. Liu, L. Shi, and J. Zi, Nat. Photon. **14**, 623 (2020).

[26] C. Huang, C. Zhang, S. Xiao, Y. Wang, Y. Fan, Y. Liu, N. Zhang, G. Qu, H. Ji, J. Han, L. Ge, Y. Kivshar, and Q. Song, Science **367**, 1018 (2020).

[27] Z. Zhang, X. Qiao, B. Midya, K. Liu, J. Sun, T. Wu, W. Liu, R. Agarwal, J. Jornet, S. Longhi, N. Litchinitser, and L. Feng, Science **368**, 760 (2020).

[28] J. Wang, M. Zhao, W. Liu, F. Guan, X. Liu, L. Shi, C. T. Chan, and J. Zi, Nat. Commun. **12**, 6046 (2021).

[29] W. Steurer and D. Sutter-Widmer, J. Phys. D: Appl. Phys. **40**, R229 (2007).

[30] A. N. Poddubny and E. L. Ivchenko, Physica E **42**, 1871 (2010).

[31] Z. V. Vardeny, A. Nahata, and A. Agrawal, Nat. Photon. **7**, 177 (2013).

[32] I. C. Fulga, D. I. Pikulin, and T. A. Loring, Phys. Rev. Lett. **116**, 257002 (2016).

[33] M. A. Bandres, M. C. Rechtsman, and M. Segev, Phys. Rev. X **6**, 011016 (2016).

[34] H. Huang and F. Liu, Phys. Rev. Lett. **121**, 126401 (2018).

[35] D. Varjas, A. Lau, K. Pöyhönen, A. R. Akhmerov, D. I. Pikulin, and I. C. Fulga, Phys. Rev. Lett. **123**, 196401 (2019).

[36] R. Chen, C.-Z. Chen, J.-H. Gao, B. Zhou, and D.-H. Xu, Phys. Rev. Lett. **124**, 036803 (2020).

[37] Z. Che, Y. Zhang, W. Liu, M. Zhao, J. Wang, W. Zhang, F. Guan, X. Liu, W. Liu, L. Shi, and J. Zi, Phys. Rev. Lett. **127**, 043901 (2021).

[38] P. Wang, Y. Zheng, X. Chen, C. Huang, Y. V. Kartashov, L. Torner, V. V. Konotop, and F. Ye, Nature (London) **577**, 42 (2020).

[39] Q. Fu, P. Wang, C. Huang, Y. V. Kartashov, L. Torner, V. V. Konotop, and F. Ye, Nat. Photon. **14**, 663 (2020).

[40] J. Zeng, Y. Hu, X. Zhang, S. Fu, H. Yin, Z. Li, and Z. Chen, Opt. Express **29**, 25388 (2021).

[41] X.-R. Mao, Z.-K. Shao, H.-Y. Luan, S.-L. Wang, and R.-M. Ma, Nat. Nanotechnol. **16**, 1099 (2021).

[42] J. B. Khurgin, Phys. Rev. A **62**, 013821 (2000).

[43] H. Tang, F. Du, S. Carr, C. DeVault, O. Mello, and E. Mazur, Light Sci. Appl. **10**, 157 (2021).

[44] J. Chen, X. Lin, M. Chen, T. Low, H. Chen, and S. Dai, Appl. Phys. Lett. **119**, 240501 (2021).

[45] K. Dong, T. Zhang, J. Li, Q. Wang, F. Yang, Y. Rho, D. Wang, C. P. Grigoropoulos, J. Wu, and J. Yao, Phys. Rev. Lett. **126**, 223601 (2021).

[46] B. Lou, N. Zhao, M. Minkov, C. Guo, M. Orenstein, and S. Fan, Phys. Rev. Lett. **126**, 136101 (2021).

[47] K. Wang, S. David, A. Chelnokov, and J. M. Lourtioz, J. Mod. Opt. **50**, 2095 (2003).

[48] M. C. Rechtsman, H.-C. Jeong, P. M. Chaikin, S. Torquato, and P. J. Steinhardt, Phys. Rev. Lett. **101**, 073902 (2008).

[49] M. Florescu, S. Torquato, and P. J. Steinhardt, Phys. Rev. B **80**, 155112 (2009).

[50] L. Jia, I. Bita, and E. L. Thomas, Phys. Rev. Lett. **107**, 193901 (2011).

[51] J.-W. Dong, M.-L. Chang, X.-Q. Huang, Z. H. Hang, Z.-C. Zhong, W.-J. Chen, Z.-Y. Huang, and C. T. Chan, Phys. Rev. Lett. **114**, 163901 (2015).

[52] H.-F. Wang, S. K. Gupta, X.-Y. Zhu, M.-H. Lu, X.-P. Liu, and Y.-F. Chen, Phys. Rev. B **98**, 214101 (2018).

[53] S. S. Sunku, G. X. Ni, B. Y. Jiang, H. Yoo, A. Sternbach, A. S. McLeod, T. Stauber, L. Xiong, T. Taniguchi, K. Watanabe, P. Kim, M. M. Fogler, and D. N. Basov, Science **362**, 1153 (2018).

[54] M. Oudich, G. Su, Y. Deng, W. Benalcazar, R. Huang, N. J. R. K. Gerard, M. Lu, P. Zhan, and Y. Jing, Phys. Rev. B **103**, 214311 (2021).

[55] J. M. B. Lopes dos Santos, N. M. R. Peres, and A. H. Castro Neto, Phys. Rev. B **86**, 155449 (2012).

[56] S. Carr, S. Fang, and E. Kaxiras, Nat. Rev. Mater. **5**, 748 (2020).

[57] V. Popescu and A. Zunger, Phys. Rev. Lett. **104**, 236403 (2010).

[58] W. Ku, T. Berlijn, and C.-C. Lee, Phys. Rev. Lett. **104**, 216401 (2010).

[59] V. Popescu and A. Zunger, Phys. Rev. B **85**, 085201 (2012).

[60] H. Nishi, Y.-I. Matsushita, and A. Oshiyama, Phys. Rev. B **95**, 085420 (2017).

[61] Y.-I. Matsushita, H. Nishi, J.-i. Iwata, T. Kosugi, and A. Oshiyama, Phys. Rev. Materials **2**, 010801(R) (2018).

[62] G. Yu, Z. Wu, Z. Zhan, M. I. Katsnelson, and S. Yuan, npj Comput. Mater **5**, 122 (2019).

[63] C. Janot, *Quasicrystals: A Primer*, 2nd ed. (Clarendon Press, Oxford, 1994), Vol. 30.

[64] P. V. C. Medeiros, S. Stafström, and J. Björk, Phys. Rev. B **89**, 041407(R) (2014).

[65] C. Lin, P. J. Steinhardt, and S. Torquato, Phys. Rev. Lett. **120**, 247401 (2018).

[66] G. Yu, Z. Wu, Z. Zhan, M. I. Katsnelson, and S. Yuan, Phys. Rev. B **102**, 115123 (2020).

[67] V. Carnevali, S. Marcantoni, and M. Peressi, Comput. Mater. Sci. **196**, 110516 (2021).

[68] Y. Zhang, M. Zhao, J. Wang, W. Liu, B. Wang, S. Hu, G. Lu, A. Chen, J. Cui, W. Zhang, C. W. Hsu, X. Liu, L. Shi, H. Yin, and J. Zi, Sci. Bull. **66**, 824 (2021).